

Kinetics Compensation Mechanism in Cosolvent Electrolyte Strategy for Aqueous Zinc Batteries

Jianlong Cong, Yueda Wang, Xing Lin, Zhimei Huang, Hua Wang, Jianbo Li, Le Hu, Haiming Hua, Jianxing Huang, Yu-Chang Lin, Henghui Xu, Zhen Li, and Yunhui Huang*



Cite This: *J. Am. Chem. Soc.* 2025, 147, 8607–8617



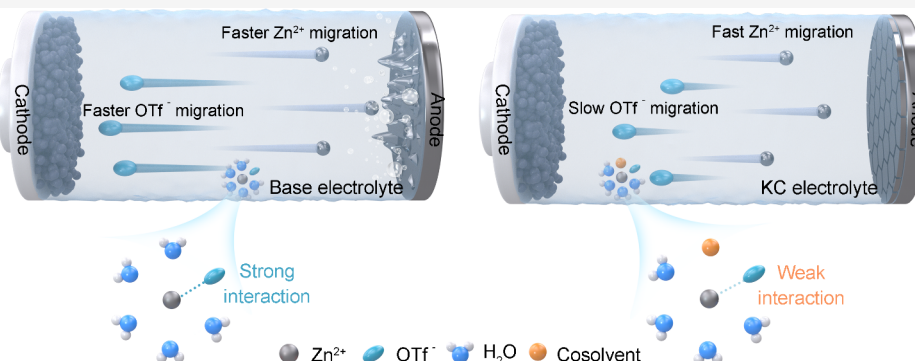
Read Online

ACCESS |

Metrics & More

Article Recommendations

Supporting Information



ABSTRACT: Aqueous zinc batteries are the ideal choices to realize intrinsically safe energy storage, but parasitic side reactions make it difficult to achieve in practice. Although the cosolvent electrolyte effectively inhibits zinc dendrites and mitigates unexpected side reactions, it brings inevitable kinetics losses. Here, we systematically investigate and compare the interactions between Zn²⁺ and various oxygen-coordinated cosolvents under pure aqueous environments and the interactions between Zn²⁺ and OTf⁻ under mixed solvent environments containing different oxygen-coordinated cosolvents. And the differences in the effect of different oxygen-coordinated cosolvents on the solvation structure of Zn²⁺ and the kinetics of ion migration are quantitatively analyzed and summarized. On this basis, we propose a new kinetics compensation mechanism in cosolvent electrolyte strategy that can compensate the kinetics losses due to the introduction of cosolvents by weakening the anion–cation pair interaction and increasing the Zn²⁺ transfer number. Theory and experiments both demonstrate that this strategy can achieve kinetics compensation of aqueous zinc batteries while improving the electrochemical performance. This work provides a comprehensive and deep understanding of designing cosolvent electrolytes with superior electrochemical performance. More importantly, the proposed strategy can be applied to other cosolvents with similar properties and other aqueous battery systems.

INTRODUCTION

Aqueous zinc batteries (AZBs) are the ideal choices to realize intrinsically safe energy storage owing to the high theoretical capacity (820 mAh g⁻¹ or 5855 mAh cm⁻³) and relatively low redox potential (−0.76 V vs standard hydrogen electrode) of Zn, high safety, and low cost.^{1–4} However, zinc dendrites and parasitic side reactions, such as hydrogen evolution reaction (HER) and corrosion, make it difficult to achieve in practice.^{5–8} To address these challenges, extensive efforts have been invested in electrolyte optimization,^{9–11} interface coating,^{12–14} separator modification,^{15,16} and host material design.^{17,18} In particular, cosolvent electrolyte effectively inhibits zinc dendrites and mitigates unexpected side reactions by regulating the solvation structure, reconstructing the hydrogen bonding network and optimizing the electric double layer (EDL) at the electrode/electrolyte interface.^{19–21} However, cosolvents are typically larger molecules and more viscous than H₂O, migrate more slowly, and thus usually incur

unavoidable kinetics losses. Moreover, the critical ion-pair distance of multivalent ions, such as Zn²⁺ and Al³⁺, is larger than that of monovalent ions, such as Li⁺ and Na⁺, which implies that multivalent ions are more likely to form anion–cation pairs and hence suffer kinetics losses.²² The effectiveness of the solvent molecule in shielding the interionic Coulombic attraction is closely related to its dielectric constant. The critical distance for the ion-pair formation q is given by the following eq 1 according to Bjerrum's treatment,

Received: December 6, 2024

Revised: February 19, 2025

Accepted: February 20, 2025

Published: March 3, 2025



Scheme 1. Schematic Illustration of Kinetics Compensation Mechanism Compared with Other Cosolvent Electrolyte Strategies

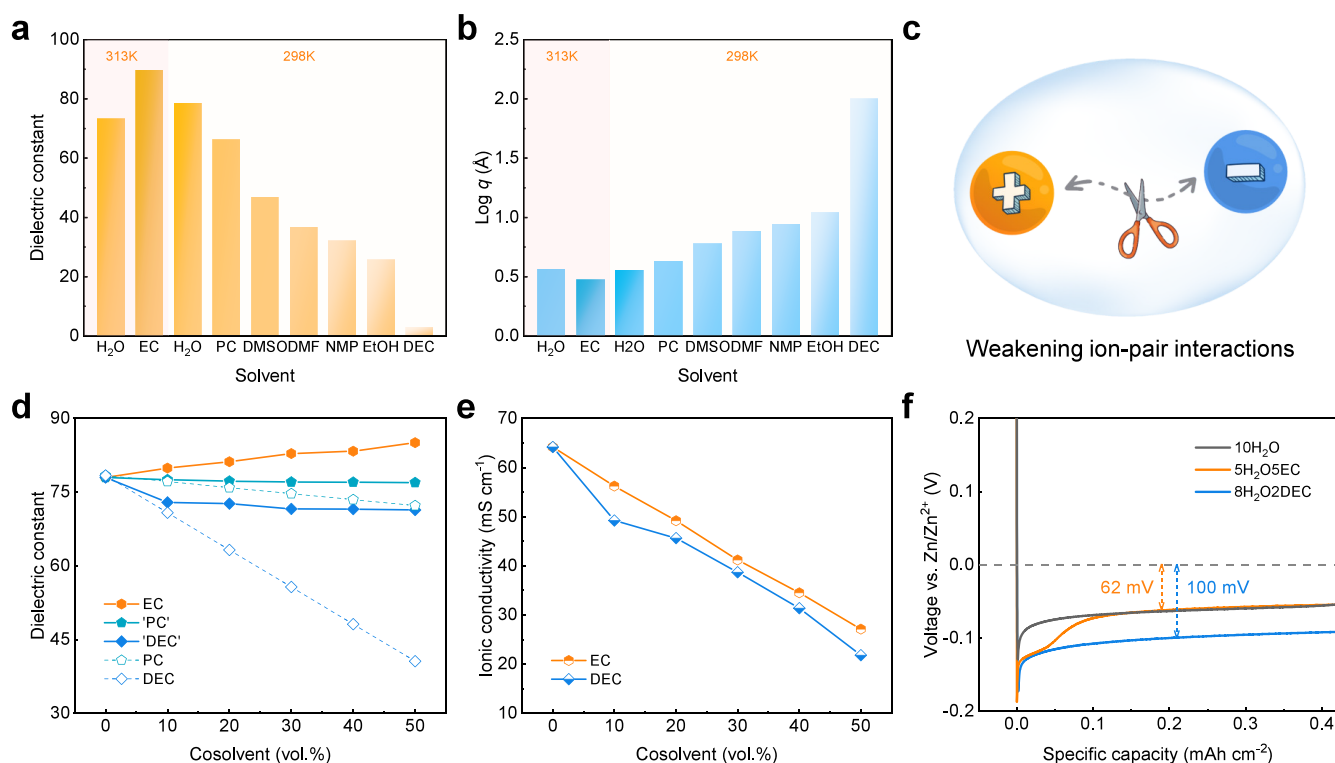
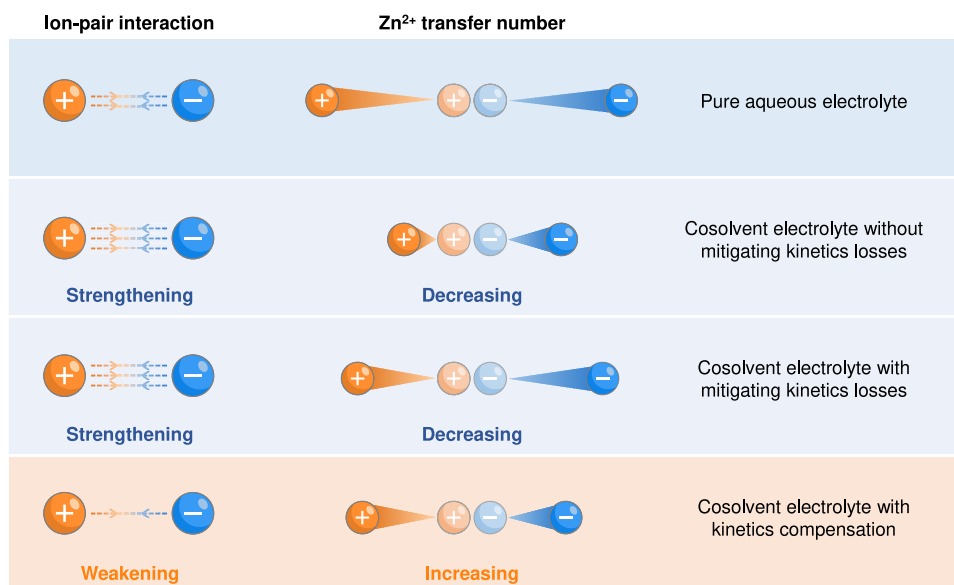


Figure 1. Differences in solvents. (a) Dielectric constant of different solvents. (b) Critical ion-pair formation distance based on monovalent ionic salts in different solvents. (c) Schematic illustration of weakening the ion-pair interaction. (d) Dielectric constant of aqueous solvents with different cosolvents. Dashed lines represent the theoretical value. (e) Ionic conductivity of 2.0 M Zn(OTf)₂ with various cosolvents. (f) Experimental voltage profiles of Zn deposition on Cu at 1.0 mA cm⁻² in different electrolytes.

with the hypothesis that ion-pair formation occurs if the interionic distance is smaller than q .²³

$$q = \frac{|z_i z_j| e^2}{8\pi \epsilon_0 \epsilon k T} \quad (1)$$

where z , ϵ_0 , k , and T are the valence orders of ions, the dielectric constant of vacuum, Boltzmann's constant, and

temperature, respectively. Therefore, for the cosolvent electrolyte, it is possible to increase the critical ion-pair distance and weaken the anion–cation pair interaction by raising the dielectric constant of mixed solvent. Moreover, the cosolvents with high dielectric constants can form the cation-dipole interaction with Zn²⁺ and regulate the solvation structure of the electrolyte, which may increase the Zn²⁺ transfer number. Weakening the anion–cation pair interaction and increasing

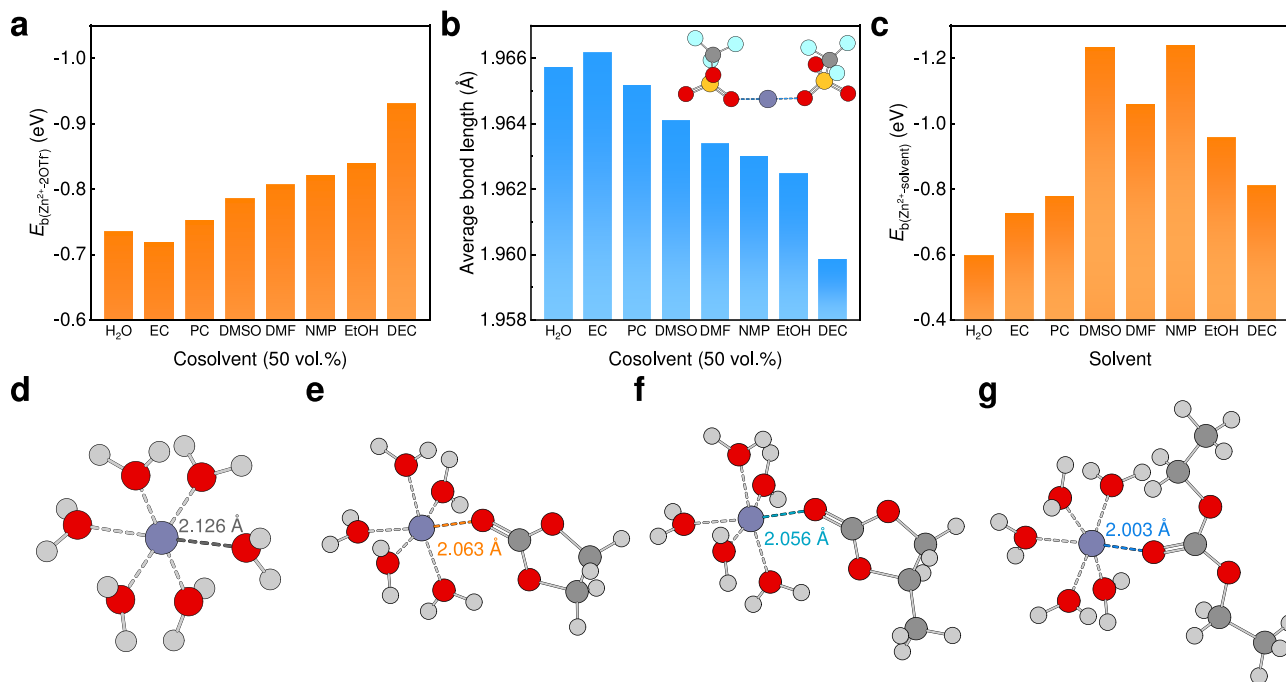


Figure 2. Interactions between components. (a) Binding energy between one Zn^{2+} and two OTf^- in pure water solvent or hybrid aqueous solvents with 50 vol % various cosolvents. (b) Average bond length between one Zn^{2+} and coordinated O atoms of two OTf^- in pure water solvent or hybrid aqueous solvents with 50 vol % various cosolvents. (c) Binding energy between Zn^{2+} and solvent molecule. (d–f) Bond length between Zn^{2+} and the coordinated O atom of (d) EC, (e) PC and (f) DEC. In the ball and stick model representation, the color scheme of atoms is H, light gray; C, dark gray; O, red, Zn, blue-gray.

the Zn^{2+} transfer number of the electrolyte can realize the kinetics compensation (KC, Scheme 1).

In this work, taking typical trifluoromethanesulfonic acid zinc ($Zn(OTf)_2$) and 7 common cosolvents as examples, we analyze the cation-dipole (Zn^{2+} -cosolvent) interactions under pure water as the implicit solvent and the ion-pair (Zn^{2+} - OTf^-) interactions under different mixed solvents as the implicit solvents by density functional theory (DFT). And it is found that the interactions between Zn^{2+} and OTf^- can be weakened by introducing the cosolvent with a higher dielectric constant than H_2O . Subsequently, we analyze the effect of introducing different cosolvents with the same volume on the first solvation shell of Zn^{2+} through molecular dynamics (MD) simulations and quantitatively analyze the differences in solvation structures and kinetics caused by the introduction of cosolvents, thereby establishing the relationship between solvation structure and kinetics performance. Finally, experiments demonstrate that the proposed cosolvent electrolyte strategy that can achieve kinetics compensation while improving the electrochemical performance of AZBs. The cosolvent electrolyte designed based on the KC mechanism achieves stable cycling of 4000 h for the Zn/Zn cell and 3000 cycles for the Zn/Cu cell at 5 $mA\ cm^{-2}$. Full cells with both synthesized cathode (K^+ doped ammonium vanadate, KNVO) and commercial cathode ($Li_{2.5}V_2(PO_4)_3$, LVP) exhibited improved electrochemical performance. Even under the extreme conditions with a low N/P ratio of 3.8 and low current density of 0.1 $A\ g^{-1}$, the Zn/LVP cell still achieves a high capacity retention of 80.4% over 200 cycles.

RESULTS AND DISCUSSION

Differences in Solvents. The solvent plays an important role in the migration kinetics of ions.²² Thanks to its small

molecular size, high dielectric constant and low viscosity, solvent water is an excellent medium for ion migration.²⁴ Among 7 kinds of common oxygenated groups solvents (ethylene carbonate (EC), propylene carbonate (PC),²⁵ dimethyl sulfoxide (DMSO),²⁶ N,N-dimethylformamide (DMF),^{27,28} N-methyl-2-pyrrolidone (NMP),²⁹ ethanol (EtOH)³⁰ and diethyl carbonate (DEC),³¹ Figure S1 and Table S1), EC is the only solvent with a higher dielectric constant than that of H_2O (Figure 1a). Therefore, although EC has a viscosity higher than that of water, the aqueous electrolytes using EC as the cosolvent may provide excellent ion migration capability by a special kinetics compensation mechanism. The critical ion-pair (q) is taken as a measure of the ion migration capacity of the electrolyte under an applied electric field.²² The subsequent calculations reveal that, except EC, all solvents exhibit a larger q value compared to H_2O (Figure 1b). This suggests that the electrolyte employing EC as the solvent can weaken the ion-pair interaction (Figure 1c).

In order to explore the impact of cosolvent mixing on the dielectric constant of hybrid aqueous solvents, we evaluated hybrid aqueous solvents with varied volume ratios of DEC, PC and EC. The dielectric constant of the hybrid aqueous solvent increases only when EC is added, as only EC possesses a dielectric constant higher than that of H_2O (Figure 1d). “DEC” and “PC” represent that the measured dielectric constants deviate from the actual values due to insufficient miscibility with water (Figure S2). Hence, a hybrid aqueous solvent containing EC can possess a superior capacity to dissociate the ion-pair. Given that the OTf^- anion comprises both hydrophilic $-SO_3^-$ and hydrophobic $-CF_3$ groups,^{31,32} miscibility between H_2O and carbonate can be achieved by introducing $Zn(OTf)_2$, enabling reliable measurement of the electrolyte’s ionic conductivity (Figure S3). Significantly, due

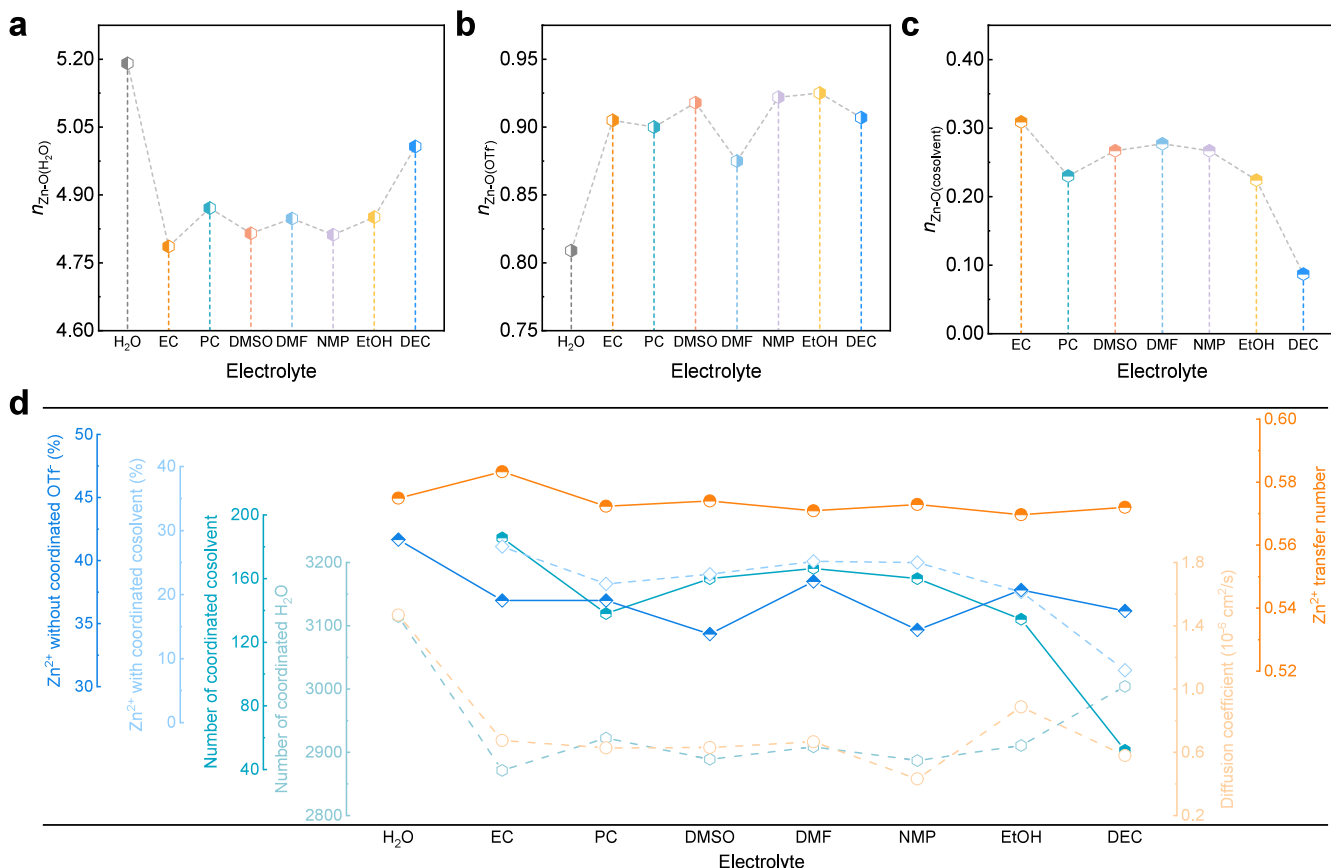


Figure 3. Differences in solvation structure. (a–c) Coordination number of the corresponding molecule/ion in the Zn^{2+} first solvation shell: (a) H_2O , (b) OTf^- and (c) cosolvents. (d) Relationship plot between the solvation environments and the kinetics properties of Zn^{2+} according to the MD results. The axes are shown in gradient height and each axis corresponds to the line chart with the same color.

to the higher dielectric constant of EC, the ionic conductivity of the electrolyte is much higher when employing the same volume of EC compared to DEC (Figure 1e), despite the higher viscosity of the electrolyte containing EC (Figure S4). Subsequently, we investigated the influence of different cosolvents on zinc electrochemical deposition (Figure S5). Although EC exhibits higher viscosity and lower ionic conductivity, we find that the deposition overpotential³³ in the 50 vol % EC aqueous electrolyte (denoted as 5H₂OSEC, the number before the solvent denotes the volume ratio, same below) is notably lower than that of the electrolyte with a smaller volume of DEC (Figure 1f), approaching the level in 2.0 M $\text{Zn}(\text{OTf})_2$ pure aqueous electrolyte. This implies the existence of a potentially unique mechanism for component interactions specific to the aqueous electrolyte using EC as a cosolvent.

Interactions between Components. To comprehend the interactions between the components in different solvent environments, we employed DFT to optimize binding configurations and then calculated the interactions between the components in detail. Strong ion-pair interaction between Zn^{2+} and OTf^- can severely weaken the ion migration capacity of the electrolyte, decreasing the Zn^{2+} transfer number.²² Hence, we first compare the interactions between Zn^{2+} and OTf^- under different hybrid solvent environments (50 vol % cosolvent, Figure 2a). The binding energy between Zn^{2+} and OTf^- in various hybrid solvents follows the order of EC < H_2O < PC < DMSO < DMF < NMP < EtOH < DEC, which inversely correlates with the dielectric constant of the

investigated solvents. This indicates that only the introduction of EC can weaken the ion-pair interaction between Zn^{2+} and OTf^- in the investigated organic solvents, while the introduction of other organic solvents strengthens the ion-pair interaction between Zn^{2+} and OTf^- . To further assess the interactions between anions and cations in diverse solvent environments, we compared the average bond length between Zn^{2+} and coordinated O atoms of two OTf^- (Figure 2b). The average bond length in hybrid solvents aligns with the order of the solvent dielectric constant, providing additional evidence that the introduction of EC effectively weakens the ion-pair interaction and enhances Zn^{2+} migration.

Subsequently, the binding energy between Zn^{2+} and various solvents was analyzed (Figure 2c). Notably, all of the organic solvents exhibit higher binding energy to Zn^{2+} than H_2O , suggesting that all introduced organic cosolvents will participate in the first solvation shell of Zn^{2+} in the aqueous electrolyte with cosolvent. Consequently, the introduction of any studied organic cosolvents will change the solvation structure of electrolyte. Furthermore, we conducted a comparative analysis of bond length between Zn^{2+} and coordinated O atoms of cosolvent or water molecules in a hexacoordinated environment (Figures 2d-g and S6). The bond lengths between Zn^{2+} and O atom of cosolvent molecules among all of the investigated cosolvents are shorter than that between Zn^{2+} and the O atom of the water molecule. This agrees with their stronger binding energy than Zn^{2+} and H_2O , and also with the smaller Mulliken charges for the coordinated O atoms (Table S2). It is worth noting that the structure

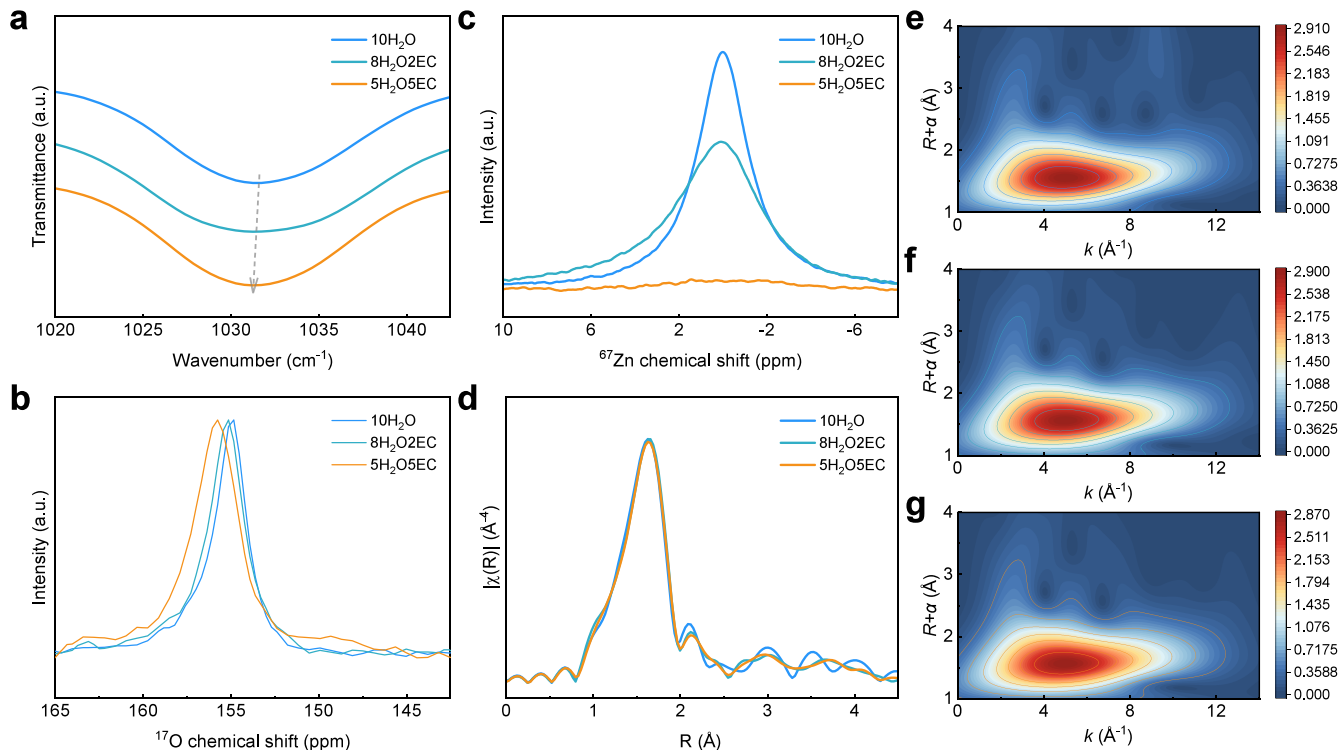


Figure 4. Effect of EC on aqueous electrolytes. (a) FTIR spectra of various electrolytes. (b) ^{17}O NMR spectra of various electrolytes. (c) ^{67}Zn NMR spectra of various electrolytes. (d) EXAFS spectra of Zn K-edge. (e–g) Wavelet transformation of Zn K-edge in (e) $10\text{H}_2\text{O}$, (f) $8\text{H}_2\text{O}2\text{EC}$ and (g) $5\text{H}_2\text{O}5\text{EC}$.

involving EC exhibits a relatively longer Zn–O bond length and relatively smaller Mulliken charge, consistent with the weaker binding energy between Zn^{2+} and EC. Additionally, electrostatic potential analysis indicates that the negative charges of the studied molecules are concentrated on the O atoms, and the electrostatic potential of the O atoms on C=O and S=O is much more negative than that of the O atoms on O–H (Figure S7). As a result, the combination of Zn^{2+} with the O atoms on C=O and S=O may lead to a larger decrease in the electrostatic potential between the cation-dipole (Figure S8 and Table S3).

Differences in Solvation Structure. The role of various cosolvents on the Zn^{2+} solvation structure in 2.0 M $\text{Zn}(\text{OTf})_2$ aqueous electrolyte was further investigated by MD simulations. To ensure comparability and reliability, we uniformly introduced 20 vol % different cosolvents into the respective electrolytes and adopted a larger system (side length approximately 8.5 nm, total atomic number approximately 60 000) for MD simulations (Table S4). The type of electrolyte is denoted by “ H_2O ” or the specific cosolvent used. In all electrolytes, MD results demonstrate that the first solvation shell of Zn^{2+} occurs within an approximate range of 2.5 Å (Figures S9–S16). All of the cosolvents successfully participate in the first solvation shell of Zn^{2+} . The radial distribution function (RDF) between Zn^{2+} and O atoms on the cosolvent ($g(r)_{\text{Zn}^{2+}-\text{cosolvent}}$) indicates that cosolvents with C=O or S=O groups exhibit a much higher probability to participate in the first solvation shell compared to cosolvents with O–H groups (Table S5). Furthermore, a significant increase is observed in all RDFs between Zn^{2+} and O atoms on H_2O ($g(r)_{\text{Zn}^{2+}-\text{H}_2\text{O}}$) upon the introduction of cosolvents, which is potentially attributed to the reduction in the number of water molecules. Remarkably, RDFs between Zn^{2+} and O atoms on OTf⁻

($g(r)_{\text{Zn}^{2+}-\text{OTf}^-}$) exhibit different degrees of increase in the electrolytes with various cosolvents, although the increase is minimal upon the introduction of EC.

We applied the coordination number to analyze the Zn^{2+} first solvation shell in detail. Upon introduction of various cosolvents into the aqueous electrolyte, a notable decrease in the number of H_2O coordinated to Zn^{2+} is observed (Figure 3a). In 2.0 M $\text{Zn}(\text{OTf})_2$ pure aqueous electrolyte, the coordination number of O atoms on H_2O is 5.19, but decreases to 4.79, 4.87, 4.82, 4.85, 4.81, 4.85, and 5.01 upon the addition of EC, PC, DMSO, DMF, NMP, EtOH, and DEC, respectively. The introduction of an equivalent volume of EC, with a dielectric constant higher than that of water, effectively minimizes the number of coordinated water molecules. Simultaneously, the number of coordinated O of OTf⁻ increases unavoidably (Figure 3b). Notably, EC has the highest number of molecules to participate in the first solvation shell of Zn^{2+} under the condition of introducing the same volume of cosolvent (Figure 3c). These results demonstrate that the introduction of EC to the aqueous electrolyte not only enhances the coordination of Zn^{2+} with the O atoms of cosolvent, but also minimizes the coordination of O atoms of H_2O as much as possible.

To gain deeper insight into the influence of cosolvents in aqueous electrolytes, we quantified the type and proportion of Zn^{2+} first solvation shells, and analyzed the ion diffusion in the electrolyte based on MD results (Figure 3d and Tables S6–S15). The results demonstrate an obvious reduction in the number of coordinated H_2O molecules with the introduction of cosolvents. This reduction is attributed to both the decrease in the solvent volume ratio occupied by H_2O molecules (from 100% to 80%) and the displacement of certain H_2O molecules by the cosolvent molecules participating in the Zn^{2+} first

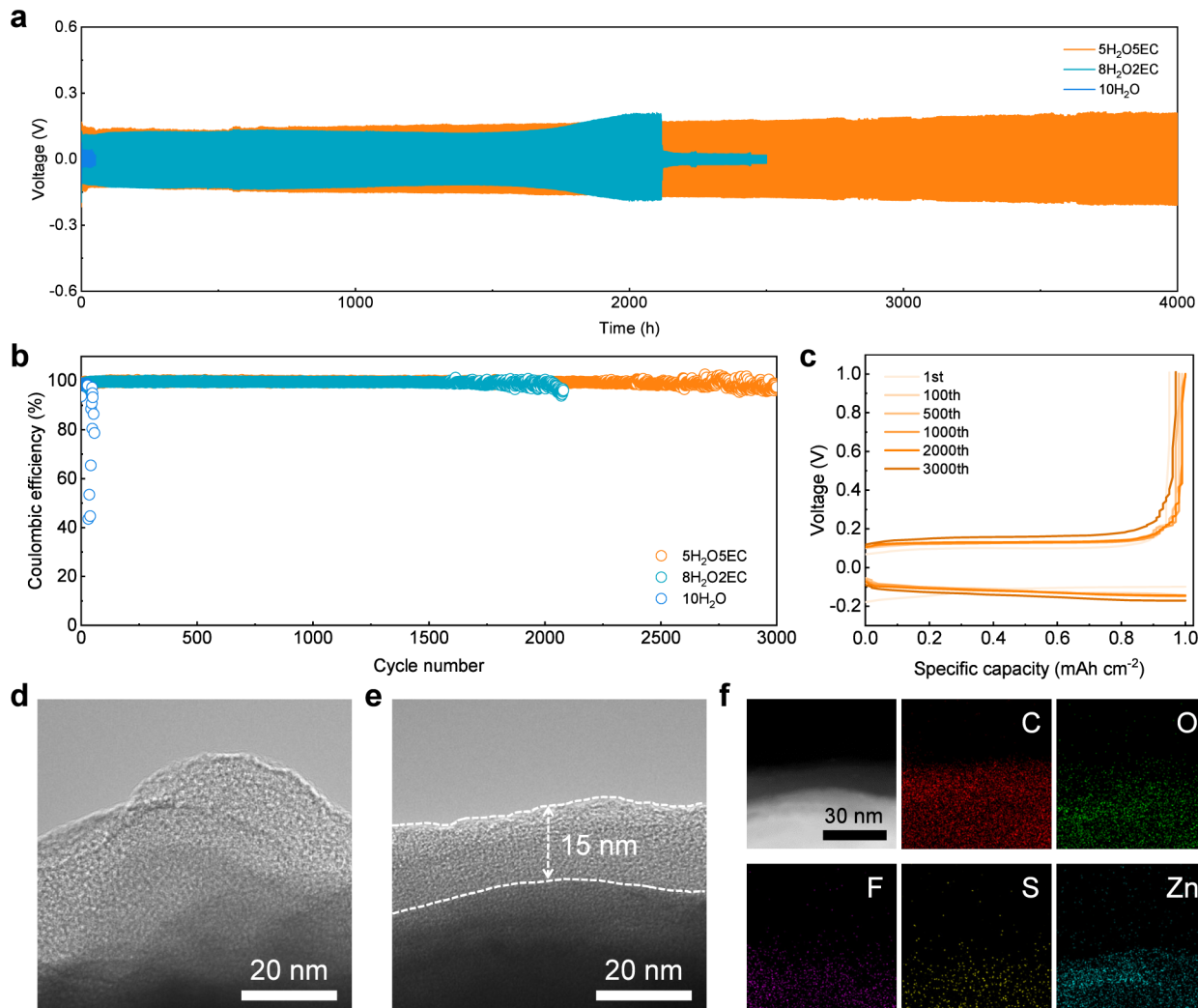


Figure 5. Electrochemical performance of KC electrolyte and Zn anode. (a) Cycle performance of Zn/Zn cells at 5.0 mA cm^{-2} and 1.0 mAh cm^{-2} . (b) Cycle performance of Zn/Cu cells at 5.0 mA cm^{-2} and 1.0 mAh cm^{-2} . (c) Corresponding voltage profiles of Zn/Cu cell in the aqueous electrolyte with 50 vol % EC. (d) HRTEM image of Zn deposited surface in pure aqueous electrolyte. (e) HRTEM image of Zn deposited surface in the aqueous electrolyte with 50 vol % EC. (f) STEM image and EDS mapping of Zn deposited surface in the aqueous electrolyte with 50 vol % EC.

solvation shell. Moreover, among all of the cosolvents, EC participates more greatly in the Zn^{2+} first solvation shell, with a higher percentage of Zn^{2+} with coordinated EC. Moreover, among all of the cosolvents, EC participates more greatly in the Zn^{2+} first solvation shell, with a higher percentage of Zn^{2+} with coordinated EC. Although the proportion of EC participating in the first solvation shell is not the highest among the investigated cosolvents in MD simulations, it is the highest among the carbonates (Figure S17). As the dielectric constant of carbonates decreases, the proportion of cosolvent participating in the first solvation shell also tends to decrease. Notably, the proportion of Zn^{2+} with coordinated cosolvent in the first solvation shell does not show a linear relationship with the dielectric constant of mixed solvents, suggesting that the ability to participate in the Zn^{2+} first solvation shell is influenced by not only the dielectric constant but also the factors such as molecular volume and type of coordinated groups.

The mean square displacement (MSD) was initially employed to assess the migration capacity of Zn^{2+} (Figure S18 and Tables S15). It is evident that the diffusion

coefficients of ions in aqueous electrolytes containing cosolvents are much smaller than that in pure aqueous electrolyte, indicating an inevitable loss of kinetics performance upon the introduction of cosolvent. Interestingly, although the diffusion coefficient of $\text{Zn}^{2+}/\text{OTf}^-$ in the electrolyte with 20 vol % EtOH exceeds that of EC, the Zn^{2+} transfer number is the highest in the electrolyte with 20 vol % EC, even surpassing that of the pure aqueous electrolyte (0.583 vs 0.575). This suggests that only introducing EC can increase the Zn^{2+} transfer number. Combined with the previous DFT results, it demonstrates that the migration kinetics of Zn^{2+} can be compensated for by weakening the ion-pair interaction and increasing the Zn^{2+} transfer number.

Effect of EC on Aqueous Electrolytes. To investigate the effect of introducing EC on aqueous electrolytes, Fourier transform infrared (FTIR) spectra were first conducted to probe the structural regularity of various electrolytes (Figures 4a and S19–S21). The peak near 1035 cm^{-1} corresponds to the OTf^- in the 2 M pure aqueous electrolytes.³⁴ And a slight red-shift occurs when the volume rate of EC increases, which suggests that the introduction of EC can regulate the

coordination environment of the OTf^- . The peak at 1773 cm^{-1} corresponds to the $\text{C}=\text{O}$ of EC and redshifts with increasing proportion of EC, indicating a subsequent increase of coordinated $\text{C}=\text{O}$. The $\text{O}-\text{H}$ stretching bands of water were recorded in the region of $3000\text{--}3800\text{ cm}^{-1}$. The $\text{O}-\text{H}$ stretching band can be classified as three types of water molecules, namely, “network water (NW)”, “intermediate water (IW)”, and “multimer water (MW)” according to the Gaussian function.^{35,36} And it can be seen that the introduction of EC interrupts the weakly H-bonded NW, which may be due to the introduction of EC affecting the interactions between water molecules.²⁵

NMR spectra was performed to investigate the interactions among H_2O , OTf^- , EC and Zn^{2+} in the aqueous electrolytes (Figures 4b-c and S22–S24). The peaks located at around 0, 155, and 200 ppm are oxygen from water, OTf^- and EC, respectively. The ^{17}O of H_2O resonance appears to downshift as cosolvents increase, suggesting enhanced shielding effect due to increased electronic density, and thus weakening the interactions between Zn^{2+} and O of water (Figure S24a). In contrast, the upshifted resonance of O from OTf^- indicates the decreased electronic density as a result of the increased ratio of OTf^- coordinated to Zn^{2+} (Figure S24b), which agrees with the MD results that the number of Zn^{2+} with coordinated O on OTf^- (Figure 3b). Compared to water, the ^{17}O resonance of pure EC appears at the higher chemical shift (Figure S22), indicating that the electronic density of ^{17}O nuclei in EC is lower than that in water.²⁵ The ^{17}O of EC resonance in electrolytes appears to upshift with the increase of EC (Figure S24c), which indicates that the EC interacting with Zn^{2+} increases. In the ^{67}Zn NMR spectra, a slight upshift can be observed as the EC increases, suggesting a decreased electronic density (Figure 4c). Besides, the broadened half peak width of ^{67}Zn relates to the slower ion migration due to the increased EC.

The effect of EC on the solvation structure was further analyzed by using X-ray absorption spectroscopy (XAS). The Zn K-edge extended X-ray absorption fine structure (EXAFS) spectra indicate a Zn–O bond length of approximately 1.63 \AA (Figure 4d), with no obvious change in either intensity or bond length for electrolytes with or without EC. Additionally, the nearly identical wavelet transform of the Zn K-edge further confirms this observation (Figure 4e-g). However, even with only 20 vol % EC, a slight change in peak shape at $2\text{--}3\text{ \AA}$ can be observed, suggesting that EC participates in the first solvation shell of Zn^{2+} .

Electrochemical Performance of KC Electrolyte and Zn Anode. To investigate the effect of EC on the electrochemical stability of electrolyte, a linear sweep voltammetry (LSV) test was first employed. It can be seen that the oxidative and reductive stability of the electrolyte increases with the amount of EC (Figures S25 and S26). In particular, the improvement in the reduction stability may be related to the suppression of water activity by decreasing the number of hydrogen bonds between water molecules (Figure S27). Tafel curves reveal that the corrosion potential (vs saturated calomel electrode, SCE) increases from -0.906 to -0.860 V , and the corrosion current decreases from 3.639 to 0.039 mA cm^{-2} with EC increasing from 0 to 50 vol % (Figure S28), which indicates that the introduction of EC can effectively improve the corrosion of the Zn anode via electrolyte and enhance the stability of the Zn anode. The flammability test indicates that even with the addition of 50 vol

% EC, the glass fiber separator soaked with electrolyte will not ignite, confirming that the aqueous electrolytes containing EC are nonflammable (Figure S29).

The electrochemical performance of the electrolyte with EC (denoted as the KC electrolyte) was first evaluated with Zn/Zn cells. The Zn/Zn cell with pure aqueous electrolyte operates for only 109 h at 1.0 mA cm^{-2} and 1.0 mAh cm^{-2} before suffering a short circuit (Figure S30). And the cycle stability of the Zn/Zn cell is much improved after introducing EC. Even with only 20 vol % EC, the cycle life of the Zn/Zn cell can be extended to 500 h. Furthermore, when EC is increased to 50 vol %, the Zn/Zn cell can operate steadily for over 2000 h without suffering short circuits. And when the current density increases to 5 mA cm^{-2} , stable plating/stripping can be maintained for more than 4000 h in the electrolyte with 50 vol % EC, compared to less than 30 h in pure aqueous electrolyte (Figure 5a). Rate performance tests indicate that Zn/Zn cells based on pure aqueous electrolyte exhibit a much higher deposition overpotential at 10.0 mA cm^{-2} due to severe side reactions such as HER and passivation of Zn anode, compared to Zn/Zn cells using the electrolyte containing EC (Figures S31 and S32). The deposition overpotential of the Zn/Zn cell using SH_2OSEC with higher viscosity and lower ionic conductivity not only is comparable to that with $8\text{H}_2\text{O2EC}$ at current densities ranging from 1.0 to 5.0 mA cm^{-2} but also matches that with a pure aqueous electrolyte. Even when the current density increases to 10.0 mA cm^{-2} , the difference in deposition overpotential between SH_2OSEC and $8\text{H}_2\text{O2EC}$ remains within 15.0 mV. This indicates that the introduction of EC not only improves the electrochemical performance of Zn anode but also confers the benefit of kinetics compensation.

Zn/Cu cells were fabricated to further analyze the cycle reversibility of the Zn anode during deposition/stripping in different electrolytes (Figure 5b). A less reversible and unstable deposition/stripping behavior is observed in pure aqueous electrolyte with lower initial Coulombic efficiency (93.7%) and average Coulombic efficiency (98.4% for 28 cycles), whereas deposition/stripping in the electrolyte with 50 vol % EC shows higher initial Coulombic efficiency (96.1%) and average Coulombic efficiency (99.7% for the first 2000 cycles, 99.4% for 3000 cycles). And the charge/discharge curves of the Zn/Cu half cells with 50 vol % EC show that the overpotential remains relatively stable over a long period of 3000 cycles (Figure 5c), suggesting excellent reversibility. Similar results are attained at 1.0 mA cm^{-2} (Figure S33), demonstrating the effectiveness of the KC electrolyte in improving the reversibility and stability of zinc deposition/stripping. Rate performance tests of Zn/Cu cells show that the deposition overpotential in SH_2OSEC is very close to that in $8\text{H}_2\text{O2EC}$ at the current densities range from 1.0 to 5.0 mA cm^{-2} (Figures S34 and S35). The former has higher viscosity and lower ionic conductivity, while the latter has lower viscosity and higher ionic conductivity. Moreover, even when the current density increases to 10.0 mA cm^{-2} , the difference between SH_2OSEC and $8\text{H}_2\text{O2EC}$ remains within 20.0 mV. This agrees with the previous rate performance test results of Zn/Zn cells and further demonstrates that the introduction of EC can achieve kinetics compensation.

To explain the stability differences in the different electrolytes, we observed the morphology of the Zn anode after cycling by using scanning electron microscopy (Figures S36 and S37). A large number of flake dendrites are formed in

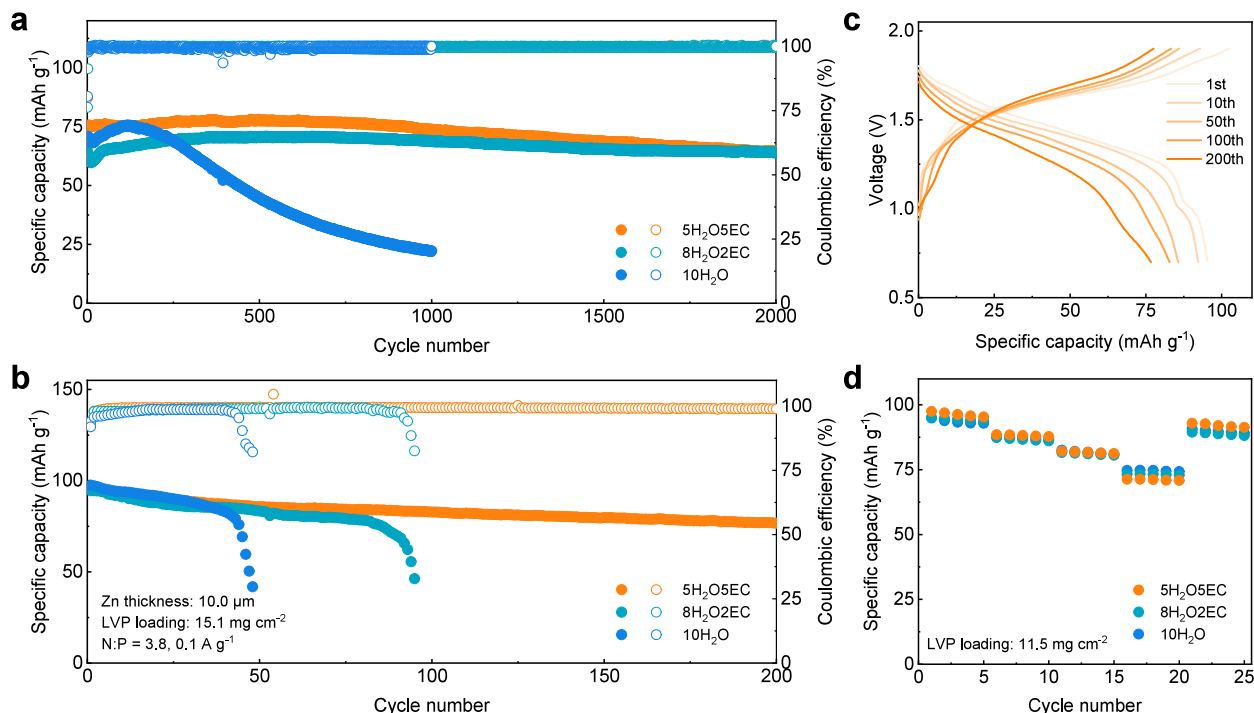


Figure 6. Electrochemical performance of full cells. (a) Cycle performance of Zn/LVP full cells at 1.0 A g^{-1} . (b) Cycle performance of Zn/LVP full cells at 0.1 A g^{-1} . (c) Corresponding voltage profiles of Zn/LVP full cells in the aqueous electrolyte with 50 vol % EC. (d) Rate performance of Zn/LVP full cells. The current densities are 0.1, 0.2, 0.3, 0.5, 0.1 A g^{-1} , respectively.

pure aqueous electrolyte, resulting in rapid short circuits in the Zn/Zn cell. In sharp contrast, a uniform and homogeneous surface is observed with 50 vol % EC. It demonstrates that the growth of Zn dendrites is effectively inhibited by introducing EC, thus improving the stability of the Zn anode during deposition/stripping. Subsequently, we investigated the microstructure of Zn deposited surface via high-resolution transmission electron microscopy (HRTEM). Compared to the Zn deposited surface in pure aqueous electrolyte (Figure 5d), a more homogeneous amorphous phase with a thickness of approximately 15 nm appears on the Zn deposited surface in the electrolyte with 50 vol % EC (Figure 5e). And low-resolution transmission electron microscopy images further reveal that the solid electrolyte interphase (SEI) formed in the electrolyte containing 50 vol % EC is more uniform, whereas the SEI in pure aqueous electrolyte is uneven and overlapped (Figure S38). The images of scanning transmission electron microscopy (STEM) and corresponding energy dispersive spectrometer (EDS) mapping indicate that the deposited Zn surface contains a large amount of C and O, and a small amount of S and F, which may originate from the partial reduction of OTf^- and EC in the first solvation shell of Zn^{2+} (Figure 5f). This provides further evidence that introducing EC is an effective way to enhance the stability of zinc anode.

Electrochemical Performance of Full Cells. To verify the effectiveness of KC electrolyte in full cells, we assembled and tested the full cells with KNVO and commercial LVP as the cathode. The microscopic morphology of synthesized KNVO is nanobelt-like (Figure S39). EDS element mappings manifest the homogeneous distribution of K, N, V and O elements in KNVO, implying the successful preintercalation of K^+ and NH_4^+ . Both peaks of $\text{NH}_4\text{V}_4\text{O}_{10}$ and $\text{K}_{0.486}\text{V}_2\text{O}_5$ are observed in the XRD pattern of synthesized KNVO, further

suggesting the successful preintercalation of K^+ and NH_4^+ ions (Figure S40).

Cyclic voltammetry (CV) tests of Zn/KNVO cells indicate that KNVO in different electrolytes exhibits two similar pairs of oxidation peaks (1.00 and 0.72 V) and reduction peaks (0.85 and 0.52 V) after an initial cycle of activation, corresponding to two pairs of charge and discharge plateaus (Figure S41). In pure aqueous electrolyte, the Zn/KNVO cell suffers rapid capacity fade with a discharge specific capacity of only 73.1 mAh g^{-1} and a capacity retention of only 49.5% after 1000 cycles (based on the maximum discharge specific capacity, 147.8 mAh g^{-1}) (Figure S42). In contrast, the Zn/KNVO cell still maintains high discharge specific capacity of 131.3 mAh g^{-1} after 2,500 cycles in the electrolyte with EC, with a capacity retention of 81.5% (based on the maximum discharge specific capacity, 161.2 mAh g^{-1}), indicating that the introduction of EC can improve the cycle stability of batteries. The corresponding charge/discharge curves provide further evidence of the previous results (Figure S43).

To investigate the effect of KC electrolyte on the cyclability of full cells at low current density, further studies were carried out using Zn/LVP cells with an LVP cathode (Figure S44 and S45). We first tested the electrochemical performance of Zn/LVP cells at a relatively high rate ($\sim 10 \text{ C}$, 1.0 A g^{-1}). It can be seen that the Zn/LVP cell in pure water electrolyte suffers a rapid capacity fade after 200 cycles (Figure 6a). In contrast, even with the addition of only 20 vol % EC, the Zn/LVP cell can cycle stably for more than 2000 cycles with a capacity retention of 90.2%. The charge–discharge curves of the full cells with different electrolytes also demonstrate that the addition of EC significantly suppresses the capacity degradation of Zn/LVP cells (Figure S46). In order to prove the potential for application under extreme conditions, we tested the cycle stability of Zn/LVP cells at low current density of 0.1

A g⁻¹ (<1 C), with 15.1 mg cm⁻² LVP as cathode, 10 μm Zn as anode and a low N/P of 3.8. The maximum actual discharge specific capacity is 102.4 mAh g⁻¹ (Figure S47). The Zn/LVP full cell in pure aqueous electrolyte suffers rapid capacity fade after 40 cycles due to anode depletion, whereas it can operate stably for 200 cycles with a capacity retention of 80.4% in the electrolyte with 50 vol % EC (Figure 6b), demonstrating that the introduction of EC can effectively improve the electrochemical reversibility and stability of full cells. And the corresponding voltage profile of the Zn/LVP full cell further proves the above conclusions (Figure 6c and S48). More importantly, the rate performance test based on the high loading LVP cathode (approximately 11.5 mg cm⁻²) reveals that the Zn/LVP cells with the aqueous electrolyte containing EC exhibit even higher discharge specific capacity due to improved reversibility (Figure 6d), although the introduction of EC inevitably leads to decreased ionic conductivity. Even at high charge/discharge rates (0.5 A g⁻¹, ~5 C), the cells still maintain discharge specific capacity extremely close to that with pure aqueous electrolyte. These results further experimentally confirm the kinetics compensation mechanism by weakening the ion-pair interaction and increasing the Zn²⁺ transfer number to enhance Zn²⁺ migration kinetics and demonstrate the potential applicability of this electrolyte design strategy.

CONCLUSIONS

We have proposed a new kinetics compensation mechanism in a cosolvent electrolyte strategy that can compensate for the kinetics losses by introducing the cosolvent with a high dielectric constant to weaken the anion–cation pair interaction and increase the transfer number. Taking a Zn(OTf)₂-based aqueous electrolyte containing EC as a model system, we validate the effectiveness of the cosolvent electrolyte strategy in achieving kinetics compensation of aqueous zinc batteries while improving the electrochemical performance. Specifically, by increasing the dielectric constant of the mixed solvent, the interaction between Zn²⁺ and OTf⁻ can be weakened and the Zn²⁺ transfer number can be increased. Quantitative analysis of MD for different cosolvents with the same volume provides a comprehensive and deep understanding on the differences and patterns of different cosolvents on the microstructure of the cosolvent electrolyte. Rate performance tests of Zn/LVP full cells demonstrate that even though the introduction of cosolvents inevitably increases the viscosity of the electrolyte and decreases its ionic conductivity, commercial cathodes with high loading can still achieve a high capacity retention at high current density, owing to kinetics compensation. Even under the extreme conditions of low N/P ratio of 3.8 and low current density of 0.1 A g⁻¹, the Zn/LVP cell still achieves high capacity retention of 80.4% over 200 cycles, demonstrating significant potential for practical application. More importantly, this strategy can also be applicable to other cosolvents with similar properties and other aqueous battery systems.

ASSOCIATED CONTENT

Supporting Information

The Supporting Information is available free of charge at <https://pubs.acs.org/doi/10.1021/jacs.4c16880>.

Experimental sections, additional figures and tables (PDF)

AUTHOR INFORMATION

Corresponding Author

Yunhai Huang – State Key Laboratory of Materials Processing and Die & Mould Technology, School of Materials Science and Engineering, Huazhong University of Science and Technology, Wuhan 430074, China;  orcid.org/0000-0003-1687-1938; Email: huangyh@hust.edu.cn

Authors

Jianlong Cong – State Key Laboratory of Materials Processing and Die & Mould Technology, School of Materials Science and Engineering, Huazhong University of Science and Technology, Wuhan 430074, China

Yueda Wang – School of Materials Science and Engineering, Hefei University of Technology, Hefei 230009, China

Xing Lin – State Key Laboratory of Materials Processing and Die & Mould Technology, School of Materials Science and Engineering, Huazhong University of Science and Technology, Wuhan 430074, China

Zhimei Huang – School of Materials Science and Engineering, Hefei University of Technology, Hefei 230009, China;  orcid.org/0000-0001-9333-8008

Hua Wang – State Key Laboratory of Materials Processing and Die & Mould Technology, School of Materials Science and Engineering, Huazhong University of Science and Technology, Wuhan 430074, China

Jianbo Li – State Key Laboratory of Materials Processing and Die & Mould Technology, School of Materials Science and Engineering, Huazhong University of Science and Technology, Wuhan 430074, China

Le Hu – State Key Laboratory of Materials Processing and Die & Mould Technology, School of Materials Science and Engineering, Huazhong University of Science and Technology, Wuhan 430074, China

Haiming Hua – State Key Laboratory of Physical Chemistry of Solid Surfaces, College of Chemistry and Chemical Engineering, Xiamen University, Xiamen 361005, China

Jianxing Huang – State Key Laboratory of Physical Chemistry of Solid Surfaces, College of Chemistry and Chemical Engineering, Xiamen University, Xiamen 361005, China

Yu-Chang Lin – National Synchrotron Radiation Research Center, Hsinchu 300092, Taiwan;  orcid.org/0000-0001-7531-9591

Henghui Xu – State Key Laboratory of Materials Processing and Die & Mould Technology, School of Materials Science and Engineering, Huazhong University of Science and Technology, Wuhan 430074, China;  orcid.org/0000-0003-2790-3122

Zhen Li – State Key Laboratory of Materials Processing and Die & Mould Technology, School of Materials Science and Engineering, Huazhong University of Science and Technology, Wuhan 430074, China;  orcid.org/0000-0003-2625-5231

Complete contact information is available at:
<https://pubs.acs.org/10.1021/jacs.4c16880>

Notes

The authors declare no competing financial interest.

ACKNOWLEDGMENTS

This work was supported by the National Natural Science Foundation of China (Grant Nos. 52027816, 52231009 and

22109003) and Guangdong Key Laboratory of Design and Calculation of New Energy Materials (No. 2017B030301013). The authors thank the Analytical and Testing Center of Huazhong University of Science and Technology (HUST), the State Key Laboratory of Materials Processing and Die & Mold Technology for characterizations and National Center for Magnetic Resonance in Wuhan.

■ REFERENCES

- (1) Zhang, N.; Chen, X. Y.; Yu, M.; Niu, Z. Q.; Cheng, F. Y.; Chen, J. Materials chemistry for rechargeable zinc-ion batteries. *Chem. Soc. Rev.* **2020**, *49* (13), 4203–4219.
- (2) Ai, Y.; Yang, C. C.; Yin, Z. Q.; Wang, T.; Gai, T. Y.; Feng, J. Y.; Li, K. L.; Zhang, W.; Li, Y. F.; Wang, F.; Chao, D. L.; Wang, Y. G.; Zhao, D. Y.; Li, W. Biomimetic Superstructured Interphase for Aqueous Zinc-Ion Batteries. *J. Am. Chem. Soc.* **2024**, *146* (22), 15496–15505.
- (3) Ruan, P. C.; Liang, S. Q.; Lu, B. G.; Fan, H. J.; Zhou, J. Design Strategies for High-Energy-Density Aqueous Zinc Batteries. *Angew. Chem.* **2022**, *61* (17), No. e202200598.
- (4) Chen, W. Y.; Wang, Y. Y.; Wang, F. M.; Zhang, Z. H.; Li, W.; Fang, G. Z.; Wang, F. Zinc Chemistries of Hybrid Electrolytes in Zinc Metal Batteries: From Solvent Structure to Interfaces. *Adv. Mater.* **2024**, *36* (47), 2411802.
- (5) Zhang, R. Z.; Pang, W. K.; Vongsivut, J.; Yuwono, J. A.; Li, G. J.; Lyu, Y.; Fan, Y. M.; Zhao, Y. L.; Zhang, S. L.; Mao, J. F.; Cai, Q.; Liu, S. L.; Guo, Z. P. Weakly solvating aqueous-based electrolyte facilitated by a soft co-solvent for extreme temperature operations of zinc-ion batteries. *Energy Environ. Sci.* **2024**, *17* (13), 4569–4581.
- (6) Xu, P. W.; Xu, M.; Zhang, J.; Zou, J. B.; Shi, Y.; Luo, D.; Wang, D. D.; Dou, H. Z.; Chen, Z. W. In-Situ Solid Electrolyte Interface via Dual Reaction Strategy for Highly Reversible Zinc Anode. *Angew. Chem.* **2024**, *63* (41), No. e202407909.
- (7) Wen, Z. P.; Hu, Z. Y.; Wang, X. W.; Zhang, Y. F.; Du, W. C.; Ye, M. H.; Tang, Y. C.; Liu, X. Q.; Li, C. C. Weakening the Space Charge Layer Effect Through Tethered Anion Electrolyte and Piezoelectric Effect Toward Ultra-Stable Zinc Anode. *Adv. Mater.* **2024**, *36* (44), 2407390.
- (8) Chen, X.; Li, W.; Reed, D.; Li, X.; Liu, X. On Energy Storage Chemistry of Aqueous Zn-Ion Batteries: From Cathode to Anode. *Electrochem. Energy Rev.* **2023**, *6* (1), 33.
- (9) Wu, H.; Hao, J. N.; Zhang, S. J.; Jiang, Y. L.; Zhu, Y. L.; Liu, J. H.; Davey, K.; Qiao, S. Z. Aqueous Zinc-Iodine Pouch Cells with Long Cycling Life and Low Self-Discharge. *J. Am. Chem. Soc.* **2024**, *146* (24), 16601–16608.
- (10) Zhou, K.; Li, Z.; Qiu, X.; Yu, Z.; Wang, Y. G. Boosting Zn Anode Utilization by Trace Iodine Ions in Organic-Water Hybrid Electrolytes through Formation of Anion-rich Adsorbing Layers. *Angew. Chem.* **2023**, *62* (39), No. e202309594.
- (11) Xiang, Z. P.; Li, Y. Y.; Cheng, X. J.; Yang, C.; Wang, K. P.; Zhang, Q.; Wang, L. Lean-water hydrogel electrolyte with improved ion conductivity for dendrite-free zinc-Ion batteries. *Chem. Eng. J.* **2024**, *490*, 151524.
- (12) Xu, Y.; Zheng, X. H.; Sun, J. F.; Wang, W. P.; Wang, M. M.; Yuan, Y.; Chuai, M. Y.; Chen, N.; Hu, H. L.; Chen, W. Nucleophilic Interfacial Layer Enables Stable Zn Anodes for Aqueous Zn Batteries. *Nano Lett.* **2022**, *22* (8), 3298–3306.
- (13) Zhao, R. Z.; Dong, X. S.; Liang, P.; Li, H. P.; Zhang, T. S.; Zhou, W. H.; Wang, B. Y.; Yang, Z. D.; Wang, X.; Wang, L. P.; Sun, Z. H.; Bu, F. X.; Zhao, Z. W.; Li, W.; Zhao, D. Y.; Chao, D. L. Prioritizing Hetero-Metallic Interfaces via Thermodynamics Inertia and Kinetics Zincophilic Metrics for Tough Zn-Based Aqueous Batteries. *Adv. Mater.* **2023**, *35* (17), 2209288.
- (14) Lv, D.; Peng, H. L.; Wang, C.; Liu, H. X.; Wang, D. D.; Yang, J.; Qian, Y. T. Rational screening of metal coating on Zn anode for ultrahigh-cumulative-capacity aqueous zinc metal batteries. *J. Energy Chem.* **2023**, *84*, 81–88.
- (15) Li, Y.; Peng, X. Y.; Li, X.; Duan, H.; Xie, S. Y.; Dong, L. B.; Kang, F. Y. Functional Ultrathin Separators Proactively Stabilizing Zinc Anodes for Zinc-Based Energy Storage. *Adv. Mater.* **2023**, *35* (18), 2300019.
- (16) Yang, H. J.; Qiao, Y.; Chang, Z.; Deng, H.; Zhu, X. Y.; Zhu, R. J.; Xiong, Z. T.; He, P.; Zhou, H. S. Reducing Water Activity by Zeolite Molecular Sieve Membrane for Long-Life Rechargeable Zinc Battery. *Adv. Mater.* **2021**, *33* (38), 2102415.
- (17) Liu, H. Z.; Li, J. H.; Zhang, X. N.; Liu, X. X.; Yan, Y.; Chen, F. J.; Zhang, G. H.; Duan, H. G. Ultrathin and Ultralight Zn Micromesh-Induced Spatial-Selection Deposition for Flexible High-Specific-Energy Zn-Ion Batteries. *Adv. Funct. Mater.* **2021**, *31* (48), 2106550.
- (18) Yu, H.; Zeng, Y. X.; Li, N. W.; Luan, D. Y.; Yu, L.; Lou, X. W. Confining Sn nanoparticles in interconnected N-doped hollow carbon spheres as hierarchical zincophilic fibers for dendrite-free Zn metal anodes. *Sci. Adv.* **2022**, *8* (10), No. eabm5766.
- (19) Yu, X. Y.; Chen, M.; Li, Z. A.; Tan, X.; Zhang, H. T.; Wang, J. H.; Tang, Y. L.; Xu, J. P.; Yin, W.; Yang, Y.; Chao, D. L.; Wang, F.; Zou, Y. G.; Feng, G.; Qiao, Y.; Zhou, H. S.; Sun, S. G. Unlocking Dynamic Solvation Chemistry and Hydrogen Evolution Mechanism in Aqueous Zinc Batteries. *J. Am. Chem. Soc.* **2024**, *146* (25), 17103–17113.
- (20) Zhong, Y. P.; Xie, X. S.; Zeng, Z. Y.; Lu, B. A.; Chen, G.; Zhou, J. Triple-function Hydrated Eutectic Electrolyte for Enhanced Aqueous Zinc Batteries. *Angew. Chem.* **2023**, *62* (40), No. e202310577.
- (21) Li, T. C.; Lin, C. J.; Luo, M.; Wang, P. J.; Li, D. S.; Li, S. Z.; Zhou, J.; Yang, H. Y. Interfacial Molecule Engineering for Reversible Zn Electrochemistry. *ACS Energy Lett.* **2023**, *8* (8), 3258–3268.
- (22) Xu, K. Nonaqueous liquid electrolytes for lithium-based rechargeable batteries. *Chem. Rev.* **2004**, *104* (10), 4303–4417.
- (23) Robertson, H.; Elliott, G. R.; Nelson, A. R. J.; Le Brun, A. P.; Webber, G. B.; Prescott, S. W.; Craig, V. S. J.; Wanless, E. J.; Willott, J. D. Underscreening in concentrated electrolytes: re-entrant swelling in polyelectrolyte brushes. *Phys. Chem. Chem. Phys.* **2023**, *25* (36), 24770–24782.
- (24) Wei, J.; Zhang, P. B.; Sun, J. J.; Liu, Y. Z.; Li, F. J.; Xu, H. F.; Ye, R. Q.; Tie, Z. X.; Sun, L.; Jin, Z. Advanced electrolytes for high-performance aqueous zinc-ion batteries. *Chem. Soc. Rev.* **2024**, *53* (20), 10335–10369.
- (25) Ming, F.; Zhu, Y.; Huang, G.; Emwas, A. H.; Liang, H.; Cui, Y.; Alshareef, H. N. Co-Solvent Electrolyte Engineering for Stable Anode-Free Zinc Metal Batteries. *J. Am. Chem. Soc.* **2022**, *144* (16), 7160–7170.
- (26) Huang, F. Y.; Li, X. P.; Zhang, Y. C.; Jie, Y. L.; Mu, X. L.; Yang, C. R.; Li, W. X.; Chen, Y. W.; Liu, Y.; Wang, S.; Ge, B. H.; Cao, R. G.; Ren, X. D.; Yan, P. F.; Li, Q.; Xu, D. S.; Jiao, S. H. Surface Transformation Enables a Dendrite-Free Zinc-Metal Anode in Nonaqueous Electrolyte. *Adv. Mater.* **2022**, *34* (34), 2203710.
- (27) Ma, Y. L.; Zhang, Q.; Liu, L. J.; Li, Y. X.; Li, H. X.; Yan, Z. H.; Chen, J. N. N-dimethylformamide tailors solvent effect to boost Zn anode reversibility in aqueous electrolyte. *Natl. Sci. Rev.* **2022**, *9* (10), nwac051.
- (28) Zou, P. C.; Lin, R. Q.; Pollard, T. P.; Yao, L. B.; Hu, E. Y.; Zhang, R.; He, Y. B.; Wang, C. Y.; West, W. C.; Ma, L.; Borodin, O.; Xu, K.; Yang, X. Q.; Xin, H. L. Localized Hydrophobicity in Aqueous Zinc Electrolytes Improves Zinc Metal Reversibility. *Nano Lett.* **2022**, *22* (18), 7535–7544.
- (29) Li, T. C.; Lim, Y.; Li, X. L.; Luo, S. Z.; Lin, C. J.; Fang, D. L.; Xia, S. W.; Wang, Y.; Yang, H. Y. A Universal Additive Strategy to Reshape Electrolyte Solvation Structure toward Reversible Zn Storage. *Adv. Energy Mater.* **2022**, *12* (15), 2103231.
- (30) Sun, Y.; Xu, Z.; Xu, X.; Nie, Y.; Tu, J.; Zhou, A.; Zhang, J.; Qiu, L.; Chen, F.; Xie, J.; Zhu, T.; Zhao, X. Low-cost and long-life Zn/Prussian blue battery using a water-in-ethanol electrolyte with a normal salt concentration. *Energy Storage Mater.* **2022**, *48*, 192–204.
- (31) Miao, L.; Wang, R.; Di, S.; Qian, Z.; Zhang, L.; Xin, W.; Liu, M.; Zhu, Z.; Chu, S.; Du, Y.; Zhang, N. Aqueous Electrolytes with

Hydrophobic Organic Cosolvents for Stabilizing Zinc Metal Anodes.
ACS Nano **2022**, *16* (6), 9667–9678.

(32) Ming, F. W.; Zhu, Y. P.; Huang, G.; Emwas, A. H.; Liang, H. F.; Cui, Y.; Alshareef, H. N. Co-Solvent Electrolyte Engineering for Stable Anode-Free Zinc Metal Batteries. *J. Am. Chem. Soc.* **2022**, *144* (16), 7160–7170.

(33) Pei, A.; Zheng, G. Y.; Shi, F. F.; Li, Y. Z.; Cui, Y. Nanoscale Nucleation and Growth of Electrodeposited Lithium Metal. *Nano Lett.* **2017**, *17* (2), 1132–1139.

(34) Alia, J. M.; deMera, Y. D.; Edwards, H. G. M.; Garcia, F. J.; Lawson, E. E. Infrared spectroscopic study of ionic association of lithium trifluoromethanesulfonate in several solvents. *J. Mol. Struct.* **1997**, *408*, 439–450.

(35) Brubach, J. B.; Mermet, A.; Filabozzi, A.; Gerschel, A.; Lairez, D.; Krafft, M. P.; Roy, P. Dependence of water dynamics upon confinement size. *J. Phys. Chem. B* **2001**, *105* (2), 430–435.

(36) Brubach, J. B.; Mermet, A.; Filabozzi, A.; Gerschel, A.; Roy, P. Signatures of the hydrogen bonding in the infrared bands of water. *J. Chem. Phys.* **2005**, *122* (18), 184509.